Coalescence limited by hydrodynamics

Vadim S. Nikolayev*

SI3M, Département de Recherche Fondamentale sur la Matière Condensée, CEA Grenoble, 17, rue des Martyrs, 38054, Grenoble Cedex 9, France; e-mail: vnikol@drfmc.ceng.cea.fr

and Daniel A. Beysens

Département de Recherche Fondamentale sur la Matière Condensée, CEA Grenoble, 17, rue des Martyrs, 38054, Grenoble Cedex 9, France (Dated: May 15, 1997)

We consider an assembly of liquid drops imbedded in another immiscible liquid of similar viscosity. It is shown that a coalescence between two drops induces another coalescence when the average distance between the drops is less than a threshold value, resulting in a "chain reaction" of coalescences. The threshold value is calculated using a "shell" model which is based on the boundary integral approach. Another, "many-drop" model is developed to test the shell approximation. We show that, although the shell model is adequate, its results can be improved by lowering the shell surface tension.

PACS numbers:

I. GROWTH BY COALESCENCE

A system formed of small droplets imbedded in a liquid is not stable. It tends to lower its total surface energy by drop coalescence, which occurs while the drops collide during their stochastic Brownian motion. The average radius of the drops grow. This model corresponds to a "diffusion-limited" growth because the time between two coalescence events is limited by diffusion of the drops. This model was first evoked in the pioneering article of Smoluchowski [1] on coagulation of colloids (see also [2] and refs. therein). The average characteristic drop size R obeys the asymptotic growth law

$$R \propto t^{1/3},\tag{1}$$

where t is time.

In contrast to this model, a purely deterministic coalescence model is discussed here. Our consideration is based on the following idea. Let us first imagine all the drops to be in vacuum rather than inside another liquid, so as to be able to neglect any interactions between them. All the drops are quiescent except two coalescing drops which form a "composite drop". If the average distance between the drops d_0 is less than a threshold value ("coalescence limit"), the composite drop will touch a neighboring drop ("drop D", Fig. 1). A second coalescence follows. The threshold value depends only on the shape of the drops and can be calculated from mere geometrical arguments.

When the drops are imbedded in another liquid, the scenario changes because of hydrodynamic interactions. The relaxing composite drop induces a flow, the direction of which is shown by the arrows in Fig. 1. This flow pushes the drop D away and hinders the second coalescence. The hydrodynamic coalescence limit should thus be less than vacuum coalescence limit.

Subsequent coalescences follow each other and the average radius of the drop pattern grows. This chain of coalescences never stops if the drop pattern is self-similar, the growth law is linear [3]:

$$R \propto t$$
. (2)

It is much faster than that (1) for the Brownian mechanism. We call this model "growth limited by hydrodynamics," because the rate of coalescence is determined by hydrodynamics. The purpose of this work is to demonstrate that a coalescence, induced by another coalescence is indeed possible and to analyze the process in detail.

The lubrication forces which prevent two interfaces from approaching are very strong. This is why the interfaces of the composite drop and the drop D would never approach without the effect of surrounding drops. In presence of the surrounding drops, the same lubrication forces act between the drop D and the surrounding drops. Then the drop D cannot be displaced strongly by the flow generated by the relaxing composite drop and the interfaces of the two

^{*} On leave from: Bogolyubov Institute for Theoretical Physics, National Academy of Sciences of Ukraine, 252143, Kiev, Ukraine

drops approach with time. We assume that when the surfaces of two drops approach each other to a distance ψ that we call the "distance of coalescence", a bridge between them forms immediately i.e., coalescence begins [4].

This retardation of the motion of the drops is due to the lubrication force which is proportional to the relative velocity of the drops. The relative velocity of the drops distant from the composite drop is proportional in turn to the velocity gradient of the fluid. The considered effect should thus be stronger inside a finite container than in an infinite system because the velocity reaches a zero value (boundary condition on the walls) at a finite distance from the composite drop and the velocity gradient is larger. Hence, if we show that a coalescence induces another coalescence in the absence of walls, it will be all the more true for the case of a finite system. The case of an infinite number of liquid drops in another liquid of infinite extent is thus considered below. The volume fraction ϕ of the droplets (ϕ = volume of drops/total volume) is however finite and can be related to d_0 . The liquids of similar large viscosities are supposed to be immiscible, and diffusion is neglected. A good example of this situation can be found in the late stages of phase separation of complex fluids and that of simple liquids, see [5] and refs. therein. Another example is the coagulation process of colloids.

A mathematical formulation for the problem is given in section II. A "shell" model for coalescences is developed in sections III,IV to calculate the hydrodynamic coalescence limit. The model is solved numerically and its results are discussed in Sec. V. We show how one coalescence induces another coalescence. In Sec. VI another simple "many-drop" model is developed. It cannot describe the second coalescence, nevertheless the validity of the shell model can be tested by comparing the results from the two models. Conclusions are given in Sec. VII.

II. HYDRODYNAMIC FORMULATION

We consider drops of a liquid phase M^+ separated from another liquid phase M^- by the interfaces ∂M , with surface tension σ . Both fluids are supposed to be incompressible and Newtonian and to have the same large shear viscosity η . These assumptions are well justified in the vicinity of a critical point of a liquid mixture. Then the problem can be treated in the creeping flow approximation. The hydrodynamic equations can be written for every point \vec{x} inside M^+ or M^- as

$$\nabla \cdot \overset{\leftrightarrow}{T} = 0, \tag{3}$$

$$\nabla \cdot \vec{v} = 0, \tag{4}$$

where \vec{v} is a fluid velocity and $\stackrel{\leftrightarrow}{T}$ is a hydrodynamic stress tensor:

$$\stackrel{\leftrightarrow}{T} = -p\stackrel{\leftrightarrow}{I} + 2\eta [\nabla \vec{v}]^s,$$

where the superscript s denotes symmetrization and \overrightarrow{I} is the unit tensor. The free boundary conditions should be specified for $\overrightarrow{x} \in \partial M$:

$$\Delta \vec{v} = 0 \tag{5}$$

$$\Delta(\overrightarrow{T} \cdot \overrightarrow{n}) = \overrightarrow{f},\tag{6}$$

 Δ denotes a difference across the surface (outer minus inner), \vec{n} is an outward normal to ∂M and \vec{f} is the force density that the fluid exerts on the interface. The force direction is opposite to Laplace's force,

$$\vec{f} = \sigma \vec{n} (\nabla \cdot \vec{n}). \tag{7}$$

The position of the interface as defined by the vector \vec{y} can be derived by the kinematic condition

$$d\vec{y}/dt = \vec{v}(\vec{y}), \quad \vec{y} \in \partial M.$$
 (8)

The motion of the fluid is assumed to be due only to the surface tension of the interface ∂M , it is then quiescent far from the interface:

$$\vec{v} \to 0 \quad \text{as} \quad |\vec{x}| \to \infty.$$
 (9)

The hydrodynamic problem (3-7), (9) can be solved explicitly [6, 7] in the integral form

$$\vec{v}(\vec{x}) = -\frac{1}{8\pi\eta} \int_{(\partial M)} \overleftrightarrow{J}(\vec{x} - \vec{y}) \cdot \vec{f}(\vec{y}) dS_y, \tag{10}$$

where

$$\overrightarrow{J}(\overrightarrow{x}) = \frac{\overrightarrow{I}}{|\overrightarrow{x}|} + \frac{\overrightarrow{x}\overrightarrow{x}}{|\overrightarrow{x}|^3}$$
(11)

is the Oseen tensor. In the case of the cylindrical symmetry of the interface ∂M one can perform an angular integration in (10):

$$v_r(r,z) = \frac{1}{8\pi\eta} \int_{(L)} dl_y [B_{rr}(r,z,r_y,z_y) f_r(r_y,z_y) + B_{rz}(r,z,r_y,z_y) f_z(r_y,z_y)],$$

$$v_z(r,z) = \frac{1}{8\pi\eta} \int_{(L)} dl_y [B_{zr}(r,z,r_y,z_y) f_r(r_y,z_y) + B_{zz}(r,z,r_y,z_y) f_z(r_y,z_y)].$$
(12)

Here L is the curve whose rotation around the z-axis generates the drop interfaces ∂M . The expressions for the non-dimensional quantities B_{ij} , i, j = r, z are presented [8] in Appendix A. Each point of L can be specified in the r-z coordinate system $(r \ge 0)$, whose axes are shown in Fig. 2. The quantities f_r , f_z are the projections of the vector \vec{f} (7) on the axes. As one can see, the surface integral in (10) is now replaced by a line integral.

The set of Eqs. 8 and 12 allows the time evolution of the interface positions to be calculated for the given initial conditions for liquid velocity and interface positions. They are defined in the next section.

III. SHELL MODEL

We aim to analyze the retardation of the motion of the drop D by the surrounding drops. As was explained in sec. I, the retardation is effective when one can find a drop (far from the composite drop) with *zero* velocity at any moment of time. Since the hydrodynamic forces decay very slowly (cf. Eq. 11) and the interdrop distance should be small to observe the effect, we need to simulate a very large number of drops, which is impossible because of prohibitively long computer times. An alternative way to demonstrate the effect with a small number of drops is to surround them by a *closed* shell which is a mean-field-like imitation of the influence of all other drops.

The chosen initial arrangement of the interfaces is shown in Fig. 2. The composite drop is an aggregate of drops that have just approached within the distance ψ . We consider another drop of radius R (drop D) at the distance d_0 from the composite drop. These two drops are enveloped by the spherical shell with the same surface tension σ as the drops (the validity of this approximation is discussed in subsection VIB). We suppose that just before coalescence takes place, the motion of the fluid is much weaker than after the coalescence (the justification of this assumption is given a posteriori in Sec. V). Thus the initial fluid velocity can then be taken to be zero everywhere. A flow in our model system is created by the composite drop which relaxes due to its surface tension and we are interested in obtaining the time t_c between two coalescences as a function of d_0 .

We have arbitrarily chosen $\psi = R/10$ in the simulation. We think that the precise definition of this distance is not relevant to the present hydrodynamic problem provided that ψ/R remains small. The value for ψ can influence the time t_c between two coalescences in two ways. On one hand, a smaller value for ψ increases the curvature of the composite drop, which then relaxes faster, thus decreasing t_c . On the other hand, the surfaces will spend more time approaching to within a smaller distance ψ , which increases t_c . One sees, at least qualitatively, that t_c can be independent of ψ . In addition, if one considers the particular case of phase separation near a critical point, scaling implies that there is only one lengthscale (R) on which depend all the variables including t_c . Hence, the latter must be independent [3] of ψ .

The setup of three spherical droplets which are arranged as shown in Fig. 2 has a low (mirror) symmetry and this arrangement requires a fairly long simulation time. This is why we chose instead, for the actual simulation, the setup of figure 2, but with a cylindrical symmetry with respect to the z axis. Then the composite drop is more like "a torus without the hole" than a dumbbell of two spheres. Such a configuration is expected to retain the main features of the real physical system since the real pattern is a complicated figure of interconnected interfaces where the drops do not resemble at all spherical objects [5]. At the very least our model system should serve to demonstrate the physical ideas presented here.

Hence, we can use (12) with the integration contour L which consists of three unconnected parts which correspond to the half contours of the drops in Fig. 2.

IV. NUMERICAL SCHEME

Even the simplified axisymmetric version of the problem remains nonlinear due to the free boundaries. Hence, a numerical method of solution is needed. The algorithm [10] with the following minor changes is used. It is possible to

avoid the rather artificial correction of the normal component of the interface velocity [10] by increasing the number of divisions of the integration contour. We checked that 400 mesh points on the contour of the composite drop (700 for all three parts of the contour) are enough to ensure that the increase of the drop volumes during the whole evolution does not exceed a few percent. The parametric integration with the trapezoidal rule is used in (12). When |dr/dz| is smaller than 5, the variable z is chosen as an integration parameter, it is r otherwise. The algorithm is not very stable, and it is necessary to maintain the distances between the mesh points approximately equal during the evolution. For this purpose a new point is added between two points (by using the three-point interpolation rule) if the distance between two points exceeds twice the average distance. Similarly, if the distance between two points becomes less than half the average distance, one point is eliminated.

V. SIMULATION RESULTS

A priori, there are two different asymptotic regimes depending on the choice of d_0 . The first corresponds to large values of d_0 when the drops relax to their spherical equilibrium shape without further coalescence. This regime takes place when reduced initial interdrop distance d_0/R exceeds a hydrodynamic coalescence limit L_H . As discussed in Sec. I, L_H is smaller than the coalescence limit in vacuum L_V . For the chosen geometry of the two drops (see Appendix B) $L_V = 0.99$.

The second regime appears when d_0/R is less than a "geometric coalescence limit" L_G . When d_0 is very small, further coalescence becomes mandatory simply because the initial shell radius R_s (which depends on d_0 , see Fig. 2) is so small that there is not enough room to contain two drops of spherical shape. It is shown in Appendix B by purely geometrical argument that in our case $L_G = 0.48$.

A question arises whether the actual value of L_H is larger than L_G . It is also interesting to know whether the new coalescence takes place between two neighboring drops or between a drop and the shell. The simulation gives answers to these questions.

We present the time evolution of the system of drops in Fig. 3. Independently of d_0 , the new coalescence takes place between the composite drop and the neighboring drop D and not between drop D and the shell. This is shown clearly in Fig. 4 where the distance between the composite and D drops (d_d) and the distance between drop D and the shell (d_s) are depicted versus time.

The result of several coalescences will therefore produce a large drop of a complicated shape. This explains the "tube-like" interconnected morphology of the growing phases which is currently observed in the experiments [5]. The most important result of the simulation is the dependence of the time lag between two subsequent coalescences (t_c) on d_0/R (Fig. 5). t_c goes to infinity for a value $d_0/R = L_H = 0.769$ which is larger than L_G . This means that the lubrication interaction with the shell (surrounding drops) slows down the drop D sufficiently to produce the second coalescence and the geometrical constraint of L_G (which is an artifact of the shell model) is irrelevant.

The time evolution of the slope of the curves in Fig. 4 reflects the time evolution of the fluid velocity in the whole space. Being initially zero (see sec. III), it rapidly achieves its maximum value and then slowly decreases to the value $v_c(\vec{x})$ at the moment of the new coalescence at $t=t_c$. Since a chain of subsequent coalescences is considered, $v_c(\vec{x})$ should be adopted as the initial condition for the fluid velocity at the beginning of the next coalescence. We consider it to be zero. This assumption is justified when d_0/R is close to L_H , which is the most interesting case. Indeed, from the definition of L_H , $v_c(\vec{x}) \to 0$ when $d_0/R \to L_H$ (Fig. 4).

It should be noted that the symmetric position of drop D in the chosen geometry can be unstable and any fluctuation may lead to its sidewise shift. However, Fig. 3 shows that the change in d_d will depend only slightly on this shift. Thus the specific geometry of our simulation should not influence t_c strongly.

Experiments [12] have shown that under the conditions of an interconnected droplet pattern, coalescence proceeds through the formation of a rim, or dimple. However, in the simulation, no dimple can be observed. Only a flattening (see Fig. 3) can be seen. This discrepancy can be understood if one considers the theoretical results [13]. They show that a dimple does not form during the coalescence of two drops when the Reynolds number is less than 1, as it is in our case.

VI. VALIDITY OF THE SHELL APPROXIMATION

It is important to know whether the influence a large number of surrounding drops can be modeled by the shell approximation as introduced in Sec. III. In this section we introduce another model and compare its results with that of the shell model.

A. Many-drop model

Since it is impossible to solve explicitly the problem of the relaxation of a composite drop surrounded by infinite number of drops, several simplifications are made which we think retain the essence of the problem:

- 1. The composite drop remains an oblate spheroid during most of the relaxation time. Its eccentricity is allowed to change.
- 2. The environment does not influence the relaxation of the composite drop, i.e. the latter moves as if it were alone.
- 3. All the drops, except the composite drop and drop D, remain spherical during the evolution. Fig. 3 shows that even drop D deforms just slightly during the evolution, which suggests that more distant drops should not deform.
- 4. The spherical drops move because of the flow imposed by the relaxing composite drop. The distance between two neighboring drops changes because of the spatial gradient of this flow. We suppose that each pair of spherical drops moves as if it were alone in a flow with a constant velocity gradient. The value of this gradient at the point where the pair is situated is calculated from the solution for the creeping flow created by the composite drop. At the same time we keep in mind that in reality, the velocity gradient vanishes at infinity.
- 5. Since the gradient is strongest along the axis of revolution of the composite drop, we consider *only* those drops whose centers are on this axis. At the beginning of the relaxation the distance l_b between their centers is supposed to be equal to the average interdrop distance which is related to the drop volume fraction ϕ .

The drops are numbered consecutively, the drop 1 (or -1 because of symmetry) corresponds to the drop D, see Fig. 6. The position of the right edge of the shell in Figs. 2 and 3 corresponds to the position of the left edge of drop 2 in Fig. 6. The aim of this subsection is to find the velocity $v^{(2)}$ of drop 2, in order to compare it with the velocity of the right edge of the shell.

The velocity field created by the relaxation of the composite drop is calculated in Appendix C for the case

$$\rho > R,\tag{13}$$

where ρ is the distance from the center of the composite drop. The results [14] are used (see Appendix D) to determine the relative velocity of the spherical drops in each pair imbedded in the gradient flow. For the relaxing oblate spheroid the maximum gradient is induced in the direction of its rotation axis (z axis, r = 0) and one can substitute into (D1) a value for g derived from the expression (C1)

$$g = \left. \frac{\partial v_z}{\partial z} \right|_{r=0} = -\frac{\sigma}{\eta} \frac{G(\varepsilon)R^2}{2\rho^3},\tag{14}$$

where G is given in (C2) as function of the eccentricity ε of the drop (see Appendix C). Since g < 0, the drops approach each other.

The simplification 4) above can be justified if

$$|\Delta g/g| < 1, (15)$$

where $|\Delta g|$ is a variation of g on the lengthscale [15] R, $\Delta g = R \mathrm{d} g/\mathrm{d} \rho$. Thus (15) yields the condition $\rho > 3R$ which is compatible with the condition (13) for the validity of the flow calculations in Appendix C. The surrounding drops move due to the flow gradient g which tends to zero as $\rho \to \infty$. Hence, we can find a drop (numbered N) whose absolute velocity $v^{(N)}$ is zero. Then

$$v^{(N-1)} = V^{(N-1)}, \quad v^{(N-2)} = V^{(N-2)} + V^{(N-1)}, \quad \dots, \quad v^{(2)} = \sum_{n=2}^{N-1} V^{(n)},$$
 (16)

where $V^{(n)}$ is the relative velocity of the drop n with respect to the drop (n+1) (cf. Eqs. D1, 14):

$$V^{(n)} = \frac{\sigma}{\eta} \frac{G(\varepsilon)R^2}{2\rho_n^3} l(n) F[R/l(n)]. \tag{17}$$

Here the function F is given by the expressions (D2) and (D3), ρ_n is a coordinate of the n-th pair of the drops

$$\rho_n = \frac{1}{2}l(n) + \sum_{i=0}^{n-1} l(i), \tag{18}$$

and l(n) is the distance between the *n*-th and (n+1)-th drops. At the beginning of the relaxation $l(n) = l_b$, see Fig. 6. Although the function l(n) is not known a priori, some useful information can be obtained, which turns out to be sufficient to calculate the upper and lower bounds for $v^{(2)}$. The distribution l(n) changes with time. Since the flow is stronger near the composite drop, l is an increasing function of n during the relaxation:

$$l(1) \le l(n) \le l(\infty) \equiv \lim_{i \to \infty} l(i). \tag{19}$$

Because the flow gradient is always zero at infinity, $l(\infty)$ does not change with time:

$$l(\infty) = l_b. \tag{20}$$

Since $(R/l)^2 F(R/l)$ is a decreasing function of l for the most important interval l > 2.2R (cf. Appendix D), (19) and (20) imply the inequality

$$v_l^{(2)} \le v^{(2)}(t) < v_u^{(2)},\tag{21}$$

where

$$v_l^{(2)} = 0.0591 \frac{\sigma}{\eta} \frac{G(\varepsilon)R^2}{l_b^2} F\left(\frac{R}{l_b}\right), \tag{22}$$

$$v_u^{(2)} = 0.0591 \frac{\sigma}{\eta} \frac{G(\varepsilon)R^2}{l^2(1)} F\left[\frac{R}{l(1)}\right]. \tag{23}$$

These expressions can be obtained [16] by using (16) with $N \to \infty$, (17 – 18), and the standard formula

$$\sum_{n=0}^{\infty} (2n+1)^{-3} = 1.05180.$$

It appears that $v_l^{(2)}$ and $v_u^{(2)}$ are functions of time because ε and l(1) also depend on time.

B. Comparison between the shell and the many-drop models

The shell model gives a number of very interesting results. However, a justification of the shell approximation is needed. We cannot compare directly the values of L_H in the shell model with that in the many-drop model because the latter cannot give a dynamic picture of coalescence, from which L_H is obtained. However, it is possible to make an indirect check of the shell model correctness by comparing the velocity of drop 2 and that of the right edge of the shell (cf. Figs. 2 and 6). These velocities should correspond to each other in the two models. We shall demonstrate here that the shell approximation yields a reasonable result and how the shell model can be improved.

First, one needs to associate the variables of both models. It is easy to establish the relations (see Figs. 2, 3 and 6)

$$l(1) = d_s + 2R$$
 and $l_b = d_0 + 2R$. (24)

The upper (23) and lower (22) bounds calculated with the substitution (24) from the simulation results appear to be very close to each other (within several percent) and thus their average can be used hereafter for $v^{(2)}(t)$.

We aim to compare $v^{(2)}$ with the velocity of the right edge of the shell in Figs. 2 and 3. Because of the symmetry of the setup in Fig. 6, the velocity of the composite drop center is equal to zero in contrast to the shell model. Hence, $v^{(2)}$ should be compared to the *relative* velocity v_s of the right edge of the shell with respect to the composite drop center.

The simulation shows that the composite drop becomes convex shortly after the beginning of its evolution (see Fig. 3). Then the drop has a degree of asymmetry two orders smaller than its oblate deformation, as can be calculated

easily from the simulation data. This justifies the simplification 1) above in the many-drop model and allows the center of the composite drop and its eccentricity ε to be determined from the shell model simulation.

The dependence of $v^{(2)}$ and v_s on ε is shown in Fig. 7. Smaller values of ε correspond to the later stages of evolution. The start of the relaxation of the composite drop, when it is not convex and cannot be approximated by a spheroid, is not shown in Fig. 7.

The comparison of $v^{(2)}$ and v_s evolutions shows that the two independent models give similar values at $\varepsilon > 0.6$. However, at small ε (late stages of evolution) the sign of v_s changes to negative i.e. the shell begins to move backwards. This is unphysical from the point of view of a many-drop system. This artifact is due to the nature of the shell: in the beginning of the evolution the shell first undergoes a prolate deformation and then relaxes because of its finite surface tension (see Fig. 3). The negative value of v_s corresponds to the relaxation.

This artifact can be suppressed by imposing to the shell a larger relaxation time, e. g. by lowering its surface tension σ_s . Since the relaxation time of the shell is given by the formula $\tau_s = \eta R_s/\sigma_s$, where R_s is the shell radius, the inequality

$$t < \tau_s \tag{25}$$

should yield the time interval where the shell behaves correctly. Fig. 7 shows that it is really so. The inequality (25) can be rewritten to give the value of σ_s which insures the correct behavior of the shell:

$$\frac{\sigma_s}{\sigma} < \frac{R_s}{R} \frac{\tau}{t},\tag{26}$$

where $\tau = \eta R/\sigma$ is the characteristic time of the drop relaxation. The minimum value of R_s (defined by (B1)) and the maximum evolution time t under consideration should be substituted into (26). For the given geometry one can choose $\sigma_s = \sigma/10$ in future simulations. This increases only slightly the coalescence time t_c ; the correction is small, as in the present simulation the shell deforms only slightly (see Fig. 3). As a matter of fact, the new value for σ_s will make L_H somewhat smaller. In other words, the corresponding value of drop volume fraction ϕ_c will be larger than that obtained from the present simulation [3] (≈ 0.26). It will thus be closer to the experimental value [5] (≈ 0.3).

It should be noted that the drawing together of the composite drop and drop D is not an artifact due to the backward motion of the shell. The comparison between the Figs. 4 and 7 shows that the drops approach each other even before the beginning of the backward motion of the shell.

The considerations of Sec. VIA can be repeated for every direction of space: only the value of g will vary. For instance, it is easy to check that the drop closest to the composite drop in the r direction (see Fig. 2) will approach it slightly, akin to the shell during the first stage of the shell deformation (while $v_s > 0$), see Fig. 3. The motion of the other nearest neighbors will also conform to the motion of the corresponding parts of the shell.

We note here that the shell velocity does not influence directly the value of L_H . Thus the poor agreement of the specific values of the velocities in Fig. 7 at small ε cannot change L_H by any significant amount.

VII. CONCLUSIONS

Two approaches to the hydrodynamically controlled coalescence have been developed. The first (the shell model) allows a detailed hydrodynamic description of a coalescence induced by a previous coalescence. This induction is possible when the average distance between the drops exceeds a critical value. This value has been calculated for a chosen geometry. A physical analysis [3] shows that the model can explain some unusual experimental facts, e.g. a linear growth law of the average size of drops (2) and an interconnected morphology of the drop pattern. At the same time, the model requires making serious simplifications: the influence of the surrounding drops is accounted for by the introduction of a spherical surface (shell) which enclose the coalescing drops. The second model, the many-drop model, is developed to examine the validity of this approximation. Although it does not give information on the motion of the coalescing drops themselves, it describes the motion of the surrounding drops. The detailed comparison of the two models shows that the shell approximation is appropriate for the description of the process of chain coalescences, both models giving the similar results in the beginning of the evolution. A shell interface tension smaller than that for the drops can be chosen to improve the shell model description at the later stages of the evolution.

Acknowledgments

V. N. would like to thank the direction of DRFMC, CEA/Grenoble for their kind hospitality and the Ministère de l'Enseignement Supérieur et de la Recherche of France for financially supporting this work.

APPENDIX A: THE EXPLICIT FORM OF THE COMPONENTS OF B

The arguments of B_{ij} are omitted for simplicity.

$$\begin{split} B_{rr} &= kr^{-3/2}r_y^{-1/2}\{-[r^2+r_y^2+2(z-z_y)^2]F + \\ &\left[2(z-z_y)^4+3(z-z_y)^2(r^2+r_y^2)+(r^2-r_y^2)^2\right]E/r_{xy}^2\}, \\ B_{rz} &= kr^{-3/2}r_y^{1/2}(z_y-z)\{F+[r^2-r_y^2-(z-z_y)^2]E/r_{xy}^2\}, \\ B_{zr} &= kr^{-1/2}r_y^{-1/2}(z-z_y)\{F-[r^2-r_y^2+(z-z_y)^2]E/r_{xy}^2\}, \\ B_{zz} &= -2kr^{-1/2}r_y^{1/2}\{F+(z-z_y)^2E/r_{xy}^2\}, \end{split}$$

where $k=2(rr_y)^{1/2}[(r+r_y)^2+(z-z_y)^2]^{-1/2}$, $r_{xy}^2=(r-r_y)^2+(z-z_y)^2$. F and E are the complete elliptical integrals of the first and second kind with modulus k.

APPENDIX B: GEOMETRIC COALESCENCE LIMIT AND COALESCENCE LIMIT IN VACUUM

For the case of the shell model, there is a geometrical criterion for the second coalescence: $d_0/R < L_G$, where L_G is calculated below. For the real case of the many-drop system there is no geometrical constraint of L_G because the closed shell is absent.

The shell radius R_s is defined by

$$R_s = R + d_0 + 2(R + d_0/2)^2 / [4(R + d_0/2)^2 - (R + \psi/2)^2]^{1/2}$$
(B1)

according to Fig. 2. If there is enough room inside the shell, the composite drop eventually becomes spherical with the radius R_c . R_c can be determined from the value of the total volume of the composite drop V_c which is conserved during the evolution:

$$R_c = (3V_c/4\pi)^{1/3}. (B2)$$

 V_c , in turn, can be calculated with sufficient accuracy as the sum of the volume of the torus and the small cylinder at its center of diameter ψ :

$$V_c = 2\pi^2 R^2 (R + \psi/2) + \pi \psi^3 / 2. \tag{B3}$$

The geometric coalescence limit can be determined from the following condition. If R_s is smaller than

$$R_s^{cr} = R_c + R + 3\psi/2,$$
 (B4)

the drops cannot avoid a point contact either between themselves or with the shell in their evolution to the equilibrium spherical shape. The value of R_s^{cr}/R can be determined explicitly from the Eqs. B2 – B4 for given ψ/R . Then one can find the corresponding value of d_0/R (i.e., the geometric coalescence limit L_G itself) by solving (B1). For $R/\psi=10$ one finds $L_G\approx 0.48$.

The coalescence limit in vacuum L_V defined in Sec. I can be found using the criterium (see Figs. 1 and 2)

$$(R_c + R + \psi)^2 + (R + \psi/2)^2 = (2R + L_V R)^2.$$
(B5)

For the chosen value of ψ it gives $L_V \approx 0.99$.

APPENDIX C: VELOCITY FIELD FAR FROM THE SPHEROIDAL DROP

First, it is necessary to reduce the expressions for B_{ij} (see Appendix A) for the case $\rho \gg \rho_y = (r_y^2 + z_y^2)^{1/2}$

$$B_{rr} = \pi r r_y^2 \rho^{-5} (2z^2 - r^2), \quad B_{rz} = 2\pi r r_y \rho^{-5} [-z\rho^2 - z_y (2z^2 - r^2)],$$

$$B_{zr} = \pi z r_y^2 \rho^{-5} (2z^2 - r^2), \quad B_{zz} = 2\pi r_y \rho^{-5} [-\rho^2 (z^2 + \rho^2) - z z_y (2z^2 - r^2)],$$

where $\rho = (r^2 + z^2)^{1/2}$ is the distance from the reference point (center of the spheroid). One needs to calculate B_{ij} within the accuracy $O[(\rho_y/\rho)^2]$, because the first approximation gives zero for velocities when the integration path in (12) is symmetric (f_z and thus the integrands are odd with respect to z_y). In this case

$$v_r = \frac{Pr}{8\eta\rho^5}(2z^2 - r^2), \quad v_z = \frac{Pz}{8\eta\rho^5}(2z^2 - r^2),$$
 (C1)

where

$$P = \int_{(L)} \mathrm{d}l_y (r_y^2 f_r - 2r_y z_y f_z).$$

For the spheroid $r^2/a^2 + z^2/b^2 = 1$ and \vec{f} from equation 7 the integration yields

$$P = \frac{b^2 \sigma}{\varepsilon^2} \left[\frac{3 + \varepsilon^2}{2\varepsilon} \ln \left(\frac{1 - \varepsilon}{1 + \varepsilon} \right) + \frac{3 - \varepsilon^2}{1 - \varepsilon^2} \right],$$

where $\varepsilon = (a^2 - b^2)^{1/2}/a$ is the eccentricity of the spheroid. The oblate spheroid can be identified with the composite drop from Fig. 2 by equalizing their volumes (cf. Eq. B3):

$$\frac{4}{3}\pi a^2 b = 2\pi^2 R^3.$$

After elimination of b, P takes the form

$$P = R^2 \sigma G(\varepsilon),$$

$$G(\varepsilon) = \frac{1}{\varepsilon^2} \left[\frac{3\pi}{2} (1 - \varepsilon^2) \right]^{2/3} \left[\frac{3 + \varepsilon^2}{2\varepsilon} \ln \left(\frac{1 - \varepsilon}{1 + \varepsilon} \right) + \frac{3 - \varepsilon^2}{1 - \varepsilon^2} \right].$$
(C2)

APPENDIX D: RELATIVE VELOCITY OF SPHERICAL DROPS IN A GRADIENT FLOW

Because the article [14] is written in Russian, we present here some of its main results. Zinchenko considers the relative motion of two liquid drops of the same radius R embedded in another fluid with the velocity field

$$\vec{v}_{\infty} = \stackrel{\leftrightarrow}{E} \cdot (\vec{x} - \vec{x}_0)$$

at infinity where \vec{E} and \vec{x}_0 are arbitrary and constant. We are interested in the particular choice of an axisymmetric flow for which the tensor \vec{E} has the form

$$\stackrel{\leftrightarrow}{E} = \operatorname{diag}(-g/2, -g/2, g),$$

and the centers of the drops lie on the z axis. In this case the relative velocity of the drops is directed along the same axis,

$$V_z = qlF, (D1)$$

where l is the distance between the drop centers and F is a function of $\alpha = R/l$. For equal fluid viscosities inside and outside the drops, the asymptotic form for F in the limit of large distance is

$$F(\alpha) = 1 - \frac{7}{2}\alpha^3 + \frac{18}{5}\alpha^5 - \frac{49}{4}\alpha^6 + O(\alpha^7).$$
 (D2)

For large α the asymptotic limit is

$$\frac{1}{F(\alpha)} = 0.690 \left(\frac{\pi^2}{16} \delta^{-1/2} - \frac{2}{9} \ln \delta + 0.559 \right) + o(1), \tag{D3}$$

where $\delta = 1/\alpha - 2$. These expressions well describe the function F, (D2) being applied for l/R > 2.2, (D3) otherwise.

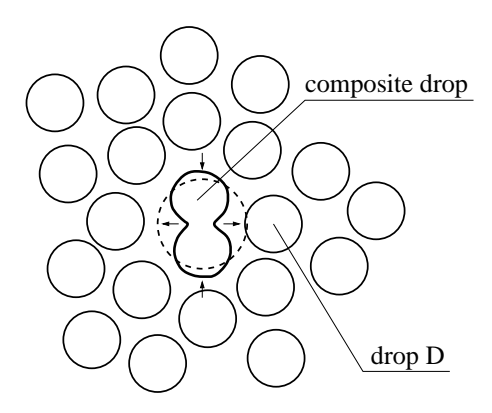


FIG. 1: Sketch of the drop pattern undergoing coalescence.

A positive value of V_z in (D1) corresponds to separating drops whereas a negative value corresponds to approaching drops.

- [1] M. von Smoluchowski, "Versuch einer matematishen Theorie dar koagulationskinetik kollider Lösungen", Z. Phys. Chem. **92**, 129 (1917).
- [2] H. Hayakawa, "Fluctuation effects in coagulation processes", Physica A 175, 383 (1991).
- [3] V. S. Nikolayev, D. Beysens & P. Guenoun, "New hydrodynamic mechanism for drop coarsening", Phys. Rev. Lett. **76**, 3144 (1996).
- [4] ψ can be defined as an effective range for attractive forces (e. g. van der Waals) which overcome the lubrication forces and, hence, make coalescence possible.
- [5] Y. Jayalakshmi, B. Khalil and D. Beysens, "Phase separation under a weak concentration gradient", Phys. Rev. Lett. 69, 3088 (1992).
- [6] D. A. Ladyzhenskaya, The Mathematical Theory of Viscous Incompressible Flow, 2nd edn., Gordon and Breach (1969).
- [7] J. M. Rallison & A. Acrivos, "A numerical study of the deformation and burst of a viscous drop in an extensional flow", J. Fluid Mech. 89, 191 (1978).
- [8] These expressions were used in [9, 10], but there were misprints in both articles. The correct formulae are presented in [11].
- [9] G. K. Youngren & A. Acrivos, "Stokes flow past a particle of arbitrary shape: a numerical method of solution", J. Fluid Mech. 69, 377 (1975).
- [10] D. Ziemanas & A. Nir, "On the viscous deformation of biological cells under anisotropic surface tension", J. Fluid Mech. 193, 217 (1988).
- [11] C. Pozrikidis, Boundary Integral and Singularity Methods for Linearized Viscous Flow, (Cambridge Univ., Cambridge, 1992).
- [12] D. Beysens, P. Guenoun, P. Sibille & A. Kumar, "Dimple and nose coalescences in phase-separation processes", Phys. Rev. E 50, 1299 (1994).
- [13] A. K. Chesters & G. Hofman, "Bubble coalescence in pure liquids", Appl. Sci. Res. 38, 353 (1982).
- [14] A. Z. Zinchenko, "Hydrodynamic interaction of two equal fluid spheres in linear flow field", Prikl. Mat. Mech. 47, 56 (1983).
- [15] It is supposed that $R \sim l_b$, i.e. the volume fraction ϕ of the drops is large.
- [16] There is a small error in the estimation of $v_u^{(2)}$ stemming from the difference between l(0) and l(1), but the accuracy is largely sufficient for the present consideration.

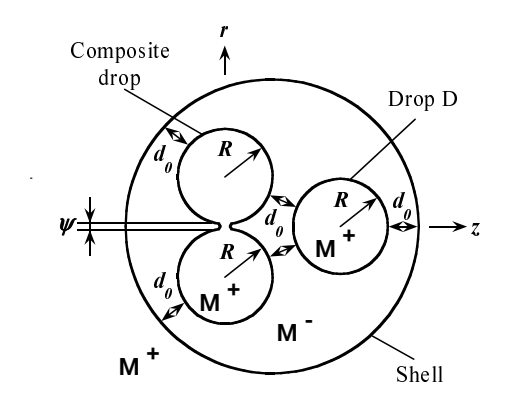


FIG. 2: Positions of the drop surfaces at the beginning of the simulation. ψ is the coalescence distance and d_0 is the initial distance between the drops.

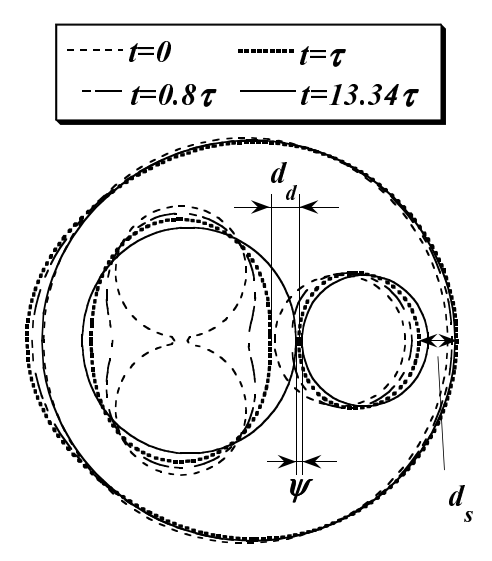


FIG. 3: Time evolution of the positions of the drop surfaces for $d_0/R = 0.65$. The second coalescence takes place at $t = t_c = 13.34\tau$, $\tau = \eta R/\sigma$. The distances between two drops d_d and between the drop D and the shell d_s are shown for the case $t = \tau$.

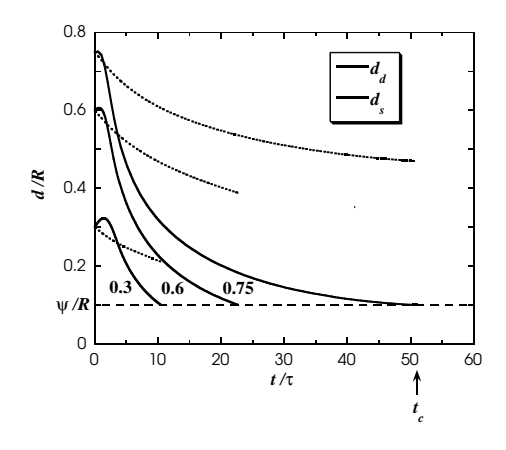


FIG. 4: Time evolution of the distances d_s and d_d for the different values of d_0/R . The distance at which the second coalescence occurs is shown as a horizontal dashed line. Coalescence time t_c is shown for $d_0/R = 0.75$. d_d grows in the beginning slightly because it is defined as a *minimum* distance between the drop surfaces. There is no growth in the dependence of the distance between the closest points of the two drops on the axis of revolution.

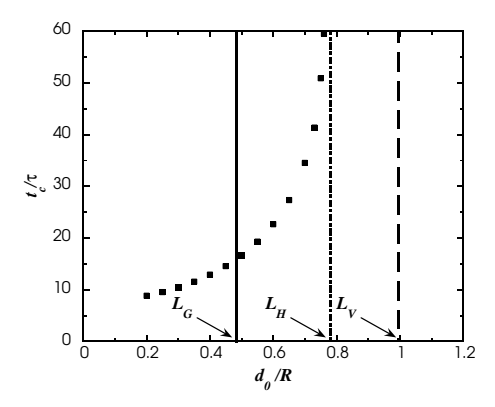


FIG. 5: Dependence of the time lag between two subsequent coalescences t_c on d_0/R , $\tau = \eta R/\sigma$. The vertical lines show the geometric and hydrodynamic coalescence limits and the coalescence limit in vacuum.

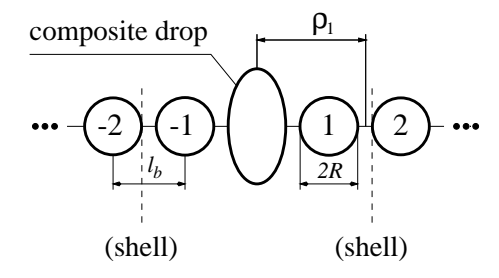


FIG. 6: Initial (equidistant) positions of the drops in the many-drop model. The distance ρ_n is shown for n=1.

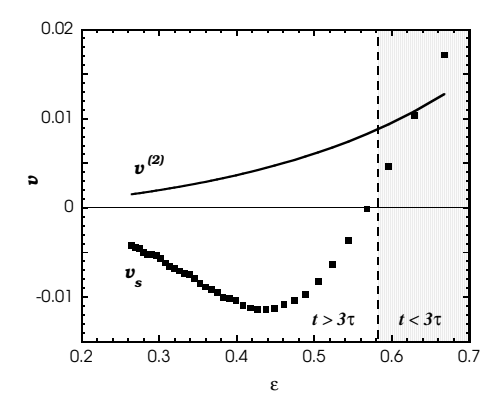


FIG. 7: Comparison of the dependencies of v_s and $v^{(2)}$ on composite drop eccentricity ε for $d_0=0.7R$ which implies $\tau_s\approx 3\tau$. A region in which the shell model gives the correct values for the drop velocities is shaded. In the shell model simulation, the composite drop reaches at $t=3\tau$ the value of eccentricity which corresponds to the boundary between two regions. The velocities are in the units σ/η .